J Sol-Gel Sci Technol (2017) 84:42–50
DOI 10.1007/s10971-017-4463-3

ORIGINAL PAPER: NANO- AND MACROPOROUS MATERIALS (AEROGELS, XEROGELS, CRYOGELS, ETC.)

# Synthesis of $SiO_2$–$W_xTiO_2$ composite aerogels via solvothermal crystallization under the guidance of bacterial cellulose followed by freeze drying method

**Dongyang Liu[1] · Fei Shi[1] · Jingxiao Liu[1] · Shicheng Hu[1] · Ling Yu[1] · Suhua Liu[1] · Yongqiang Wang[1] · Zhengjie Shan[1] · Jia Liu[1] · Xiaomei Tian[1]**

Received: 6 April 2017 / Accepted: 1 July 2017 / Published online: 31 July 2017


**Abstract** In order to obtain aerogel-based photocatalytic materials with higher adsorptivity and photocatalytic activity, $SiO_2$–$W_xTiO_2$ composite aerogels were synthesized by the method of combining freeze drying with solvothermal crystallization under the guidance of bacterial cellulose using BC–$SiO_2$ composite gel as skeleton. The influences of W/Ti mol ratio, solvothermal process parameters on the microstructure and properties of the $SiO_2$–$W_xTiO_2$ composite aerogels were investigated. The results indicate that the obtained composite aerogels have higher specific surface area with 297–377 $m^2 g^{-1}$ and pore volume with 0.46–0.66 $cm^3 g^{-1}$. The adsorption/photocatalysis test indicates that the obtained aerogels showed prominent adsorption/photocatalytic activity, and the adsorption/photocatalytic degradation rate for Rhodamine B in aqueous solution could attain to 95 % within 120 min, which is obviously better than that of P25. With the increase of solvothermal crystallization time, the adsorption/photocatalysis tends to increase and the $SiO_2$–$W_xTiO_2$ composite aerogel sample exhibited better removing efficiency for Rhodamine B. Doping of 2–3% W is favorable for improving the adsorption/photocatalytic properties of the $SiO_2$–$W_xTiO_2$ composite aerogels.

**Graphical abstract** The $SiO_2$–$W_xTiO_2$ composite aerogels were synthesized by the method of combining freeze drying with solvothermal crystallization under the guidance of bacterial cellulose (BC). The presence and hydrolysis of BC as a template and inducer during the solvothermal process played an important role in enhancing the porous network structure of the composite aerogels and inducing the deposition/crystallization of $W_xTiO_2$ nanoparticles. The $SiO_2$–$W_xTiO_2$ composite aerogels exhibited higher adsorptivity and photocatalytic activity simultaneously.

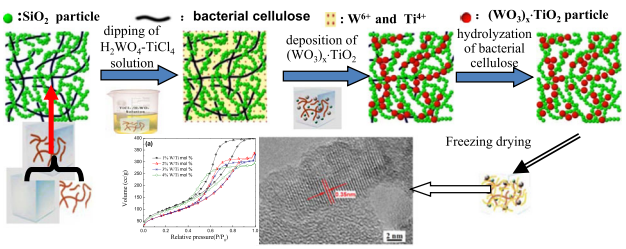


**Keywords** Composite aerogel · $SiO_2$–$W_xTiO_2$ · Bacterial cellulose (BC) · Solvothermal crystallization · Freeze drying · Photocatalytic activity/poperties

## 1 Introduction

As is well known, titania has excellent ultraviolet (UV) photocatalytic properties, and its photocatalytic efficiency can be improved further by adjusting its specific surface area, crystallinity and band gap energy [1–5]. It is reported that the recombination time of photo-generated electron-hole of $TiO_2$ can be extended by doping other metal ions or combining with other oxide semiconductor so as to further

✉ Fei Shi
shifei@dlpu.edu.cn

✉ Jingxiao Liu
drliu-shi@dlpu.edu.cn

[1] Key Laboratory of New Materials and Modification of Liaoning Province, School of Textile and Materials Engineering, Dalian Polytechnic University, Dalian 116034, PR China

improve its photocatalytic efficiency or photocatalysis in the visible light region [6–10]. Because the conduction band of $WO_3$ is lower than that of $TiO_2$, the coupling of them is beneficial to the electron transition to the conduction band of $TiO_2$, which causes the improvement of the quantum efficiency and photocatalytic performance in the visible light region [11–14]. In our previous research [15], the hydrothermal synthesis of $WO_3$–$TiO_2$ particles was investigated, and the results indicated that the sample with 2 mol %$WO_3$–$TiO_2$ exhibited best photocatalytic properties.

Apart from photocatalysis, adsorption is another powerful strategy for environmental purification. Silica arogels are unique mesoporous materials with higher specific surface area, large pore volume and excellent adsorption ability, and thus can be widely used in the adsorption of harmful pollutants in the air and water [16–18]. As is reported, preparation of $TiO_2$–$SiO_2$ composite aerogels is favorable for achieving higher removing efficiency for harmful pollutants in the environment due to the synergistic promotion effect of adsorption and photocatalysis. In the last few years, $TiO_2$–$SiO_2$ composite aerogel materials have attracted much attention because they have broad application prospects in the field of environmental purification [19–21]. The usual method of preparing $TiO_2$–$SiO_2$ composite aerogel is mixing $TiO_2$ sol or $TiO_2$ powders directly with $SiO_2$ sol to get composite sol-gel and then using different drying method to obtain the composite aerogel products [22–24]. However, it is difficult to obtain the composite aerogel with higher $TiO_2$ content and crystallinity by conventional sol–gel and surface modification/ambient pressure drying method [25]. Zu et al. [26] synthesized $TiO_2$–$SiO_2$ composite aerogels by chemical liquid deposition and supercritical drying method, in which the $SiO_2$ wet gel was immersed in the partially hydrolyzed titania alkoxides sol for a period of time to deposit $TiO_2$ nanoparticles in the network of $SiO_2$ gel. Nevertheless, additional heat treatment was still required to further improve the crystallinity of $TiO_2$, and the supercritical drying method is not ideal for production on a large scale owing to the long preparation period, low yield and high-cost.

Recently, bacterial cellulose (BC) has been attracting great interest in synthesizing mesoporous aerogel-based materials as template. BC is different from traditional segmented copolymer, it is a kind of special biological polymer gel with three-dimensional network structure formed by microfiber [27–29]. Sai et al. [30] prepared flexible and crack-free BC– $SiO_2$ composite aerogels by sol–gel and freeze drying method, and it was found that the obtained BC–$SiO_2$ composite aerogels showed excellent robustness and flexibility due to the synergic effects of the BC matrix and $SiO_2$ gel skeleton. It was also reported that lightweight porous magnetic aerogels could be prepared by using the freeze-dried BC nanofibril aerogels as template for the growth of cobalt ferrite nanoparticles [31]. Thus, it can be expected that using a combined network structure of $SiO_2$ gel with functional template BC as the skeleton of $TiO_2$ deposition and combining with solvothermal crystallization may be more favorable for obtaining composite aerogels with higher pore volume and higher $TiO_2$ content and crystallinity. However, synthesis of photocatalyst-$SiO_2$ composite aerogel by the method of combining freeze drying with solvothermal crystallization under the guidance of BC has not been reported yet.

Therefore, in this study, $SiO_2$–$W_xTiO_2$ composite aerogels have been prepared by freeze drying method using BC–$SiO_2$ composite gel as precursor via soaking of $WO_3$–$TiO_2$ solution and solvothermal crystallization. The effects of the W/Ti molar ratio and solvothermal crystallization process on the microstructure and properties of the composite aerogels were investigated. The mechanism of forming photocatalyst–$SiO_2$ composite aerogels with higher pore volume and crystallinity through solvothermal crystallization followed by freeze drying method was discussed. The synthesis method in this work is of great reference value for preparing other kinds of photocatalyst–$SiO_2$ composite aerogels, and the as-prepared $SiO_2$–$W_xTiO_2$ composite aerogels will have a broad application prospect in the field of wastewater treatment and air purification.

## 2 Experimental

### 2.1 Preparation of BC–$SiO_2$ composite gel

First, the BC (ShangHai YiFang Rural Technology Holdings Co. Ltd) was heated in a concentrated 2 M KOH solution and was washed repeatedly with deionized water so as to remove sugar. Then, it was made into paste with a juicer.

The water glass was diluted with deionized water (the volume ratio of water glass/deionized water = 1:6), and then was ion exchanged with 732 cation exchange resin to obtain silica acid with pH = 2–3. BC was mixed with silica acid with the volume ratio of BC/silica acid = 1:10. After vigorous stirring for 10 min, gelation of BC/silica acid mixture occurred and the BC–$SiO_2$ composite gel was obtained after aged for 2 h.

### 2.2 Preparation of $SiO_2$–$W_xTiO_2$ composite aerogels

First, The $WO_3$–$TiO_2$ precursor solution was prepared with the molar ratio of W/Ti = 1–5% by adding a certain amount of 0.5 mol/L $H_2WO_4$ solution into the 3 mol/L $TiCl_4$ solution and stirring for 30 min. Then, the above obtained BC–$SiO_2$ composite gels were divided into small pieces with about 1 $cm^3$ and were immersed in equal volume

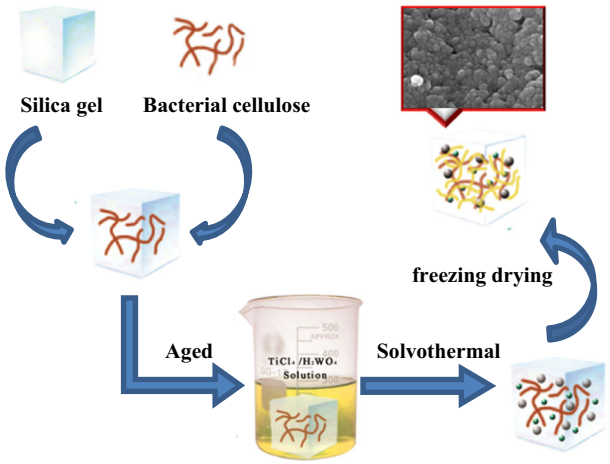


**Fig. 1** The flow chart of preparing $SiO_2$–$W_xTiO_2$ composite aerogels

$WO_3$–$TiO_2$ solution for 24 h to obtain $SiO_2$–$W_xTiO_2$ composite gels. After transferring the composite gels with 100 ml ethanol into a 200 ml Teflon-lined autoclave, the solvothermal crystallization was carried out at 100 or 180 °C for 3–51 h. Finally, the obtained white $SiO_2$–$W_xTiO_2$ composite gels were freeze dried for 20 h to obtain $SiO_2$–$W_xTiO_2$ composite aerogels. Figure 1

### 2.3 Characterization

The surface groups of the obtained $SiO_2$–$W_xTiO_2$ composite aerogels were analyzed by FT-IR/NIR Spectrometer (Spectrum two, PerkinElmer, US). The phase and structure of composite aerogels were characterized by X-ray diffractometer (XRD-7000, SHMADZU, Japan) using Cu anode target, tube voltage 40 kV, tube current 45 mA, scanning range 15–80°. The thermal evolution process of bacterial cellulose and composite aerogels was studied by the differential thermal analyzer (DTA, WCR-2D, Beijing Optical Instrument Factory). A field emission scanning electron microscopy (FESEM, JEOL JSM-7800F, Japan) and transmission electron microscope (TEM, JEOL JEM-2100UHK, Japan) were used to observe the surface morphology and microstructure of the composite aerogels. The pore structure of composite aerogels was characterized by $N_2$ adsorption–desorption specific surface area analyzer (SSA-4200, BJbuilder, China). The specific surface area of the sample was calculated from $N_2$ physisorption Brunauer–Emmet–Teller (BET) equation, and the pore volume and pore size distribution of the samples were obtained by Barrett–Joyner–Halenda (BJH) model in the desorption stage. The Ultraviolet–Visible (UV–Vis) absorption spectra was measured by UV–VIS Spectrophotometer (Lambda35, PerkinElmer, US).

The organic dyes Rhodamine B (RhB) was used for evaluating the adsorption/photocatalysis capability of the

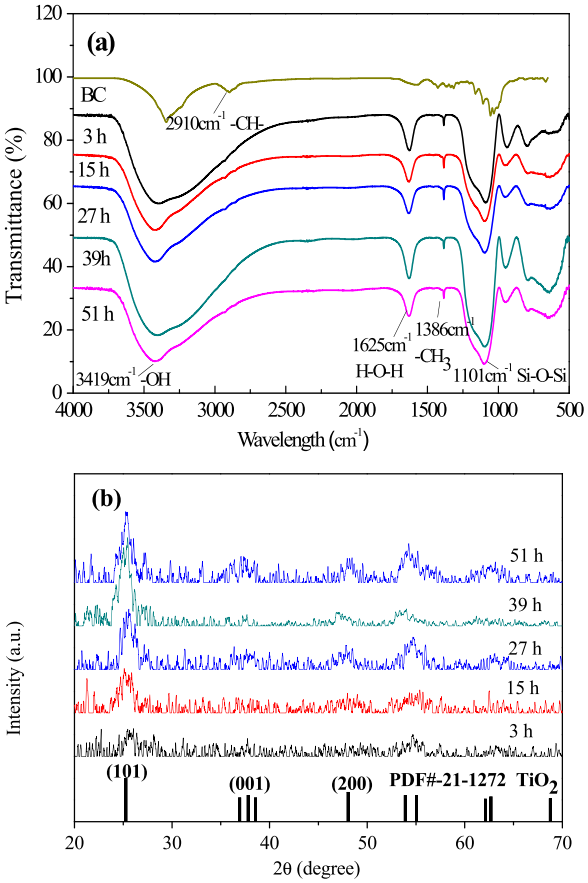


**Fig. 2** FTIR spectra **a** and XRD patterns **b** of $SiO_2$-2mol%$W_xTiO_2$ composite aerogels with different solvothermal crystallization time at 100 °C

$SiO_2$–$W_xTiO_2$ composite aerogels. First, 0.1 g composite aerogel samples were added into a 250 ml beaker with 100 ml $1 \times 10^{-5}$ M RhB solution together. During the adsorption experiment, the RhB solution was stirred in dark environment. At regular intervals, the upper clear supernatant liquid was measured using UV–Vis spectrophotometer (UV751 GD) at wavelength 554 nm. After 60 min of adsorption, the photocatalytic capability was determined by the optical absorbance of the solution after high pressure mercury lamp (the output power was 125 W, K > 400 nm) irradiation for different time, with the distance between reactor and light source being about 64 cm.

## 3 Results and discussion

Figure 2a shows the IR spectra of BC and the synthesized $SiO_2$-2mol%$W_xTiO_2$ composite aerogels with solvothermal crystallization at 100 °C for different time. It is evident that apart from the Si-O-Si group (absorption peak at about 1101 $cm^{-1}$), hydrophilicity of the composite aerogels can be verified by the absorption peaks at 3419 and 1625 $cm^{-1}$,

which corresponds to the stretching of -OH and deformation of H-O-H groups, respectively. Additionally, there is no significant change in the infrared spectra with the increase of solvothermal time. However, by comparison with the BC, there is no peak at 2910 $cm^{-1}$ corresponding to -CH- groups in the spectra of composite aerogels, which indicates that the BC chains decomposed during the solvothermal crystallization.

Figure 2b shows the X-ray diffraction (XRD) patterns of the synthesized $SiO_2$–2mol%$W_xTiO_2$ composite aerogels with different solvothermal crystallization time at 100 °C. All the XRD patterns have diffraction peaks at 25.3°, 37.8° and 48.0°, which correspond to (101), (001) and (200) of anatase $TiO_2$ crystal phase (standard spectrum PDF No. 21-1272), respectively. It is obvious that the composite aerogels after freeze drying with solvothermal crystallization at 100 °C exhibited obvious anatase $TiO_2$ crystal phase, but its crystallinity is not high. With the extension of the solvothermal crystallization time, the crystallinity of anatase $TiO_2$ crystal increased gradually, but the composite aerogels prepared by solvothermal deposition for 51 h at 100 °C exhibited still a lower crystallinity.

In order to further improve the crystallinity of anatase $TiO_2$ in $SiO_2$–$W_xTiO_2$ composite aerogels, the temperature of solvothermal crystallization was increased to 180 °C. The XRD patterns of the synthesized $SiO_2$–$W_xTiO_2$ composite aerogels by solvothermal crystallization for 3 h at 180 °C with different W/Ti molar ratio is shown in Fig. 3. It can be seen that all of the synthesized $SiO_2$–$W_xTiO_2$ composite aerogels with solvothermal crystallization for 3 h at 180 °C exhibit higher crystallinity. The diffraction peaks corresponding to (101), (001) and (200) of anatase $TiO_2$ crystal phase have a slight shift, which suggests that the incorporation of a small amount of W causes the lattice structure of anatase $TiO_2$ slightly changed. However, due to the extremely low content of $WO_3$, the diffraction peak of $WO_3$ crystal phase is not reflected in the XRD spectra.

The DTA curves of BC and the synthesized $SiO_2$–2mol% $W_xTiO_2$ composite aerogels with solvothermal crystallization for 3 h at 180 °C are shown in Fig. 4. It is obvious that the exothermic peak at 313 °C in the DTA curve of the BC is due to the decomposition of BC. However, the DTA curve of the composite aerogel using BC as template has a similar exothermic peak about 254 °C with the composite aerogel without BC as template, indicating that there is no BC in the composite aerogels because of hydrolysis of BC to glucose group in the network during solvothermal crystallization. The exothermic peak at 254 °C corresponds to the decomposition of the glucose group. It is suggested that the hydrolysis of BC during the solvothermal crystallization is not only favorable for achieving higher pore volume of composite aerogel, but also beneficial to the deposition and growth of $W_xTiO_2$ particles. That is the main reason that

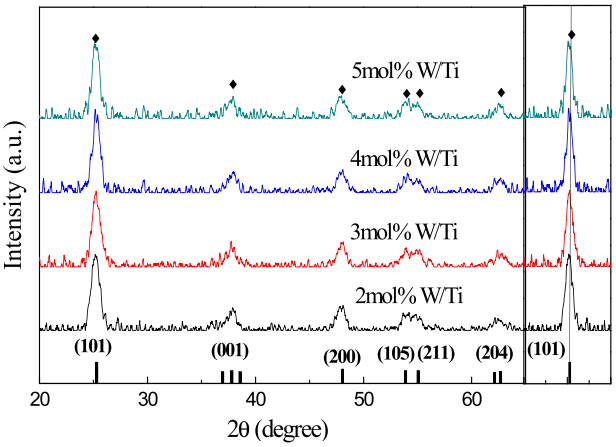


**Fig. 3** XRD patterns of the $SiO_2$–$W_xTiO_2$ composite aerogels with solvothermal crystallization for 3 h at 180 °C and different W/Ti molar ratio

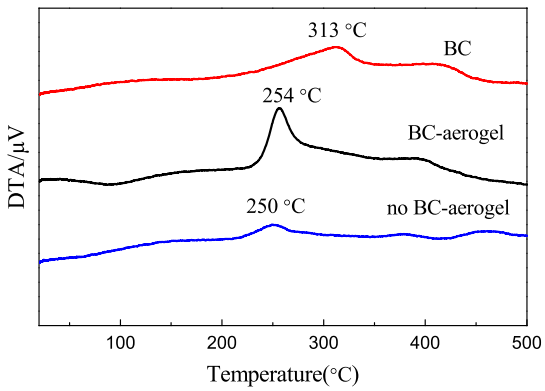


**Fig. 4** DTA curves of BC and the synthesized $SiO_2$–2mol%$W_xTiO_2$ composite aerogels with solvothermal crystallization for 3 h at 180 °C with and without using BC as template

$SiO_2$–$W_xTiO_2$ composite aerogels with higher pore volume and $TiO_2$ crystals content could be obtained by the subsequent freeze drying method.

Figure 5 shows the SEM images of the $SiO_2$–$W_xTiO_2$ composite aerogels synthesized with different solvothermal condition and W/Ti molar ratio. It can be seen that the synthesized composite aerogels contains 20–30 nm spherical clusters and pores less than 10 nm between them. The extension of the solvothermal crystallization time resulted in the tendency of the particles growing up (Fig. 5a–b). On the other hand, the W/Ti molar ratio has no significant effect on the size of the composite aerogel particles (Fig. 5c–d).

Figure 6 shows the TEM images of pure $SiO_2$ aerogels without $W_xTiO_2$ deposition and the synthesized $SiO_2$–2mol% $W_xTiO_2$ composite aerogels with solvothermal crystallization for 3 h at 180 °C. The sample pure $SiO_2$ aerogel in Fig. 6a, b was prepared by solvothermal treatment of the precursor BC–$SiO_2$ composite gel under the same pH conditions with the $SiO_2$–$W_xTiO_2$ composite aerogels

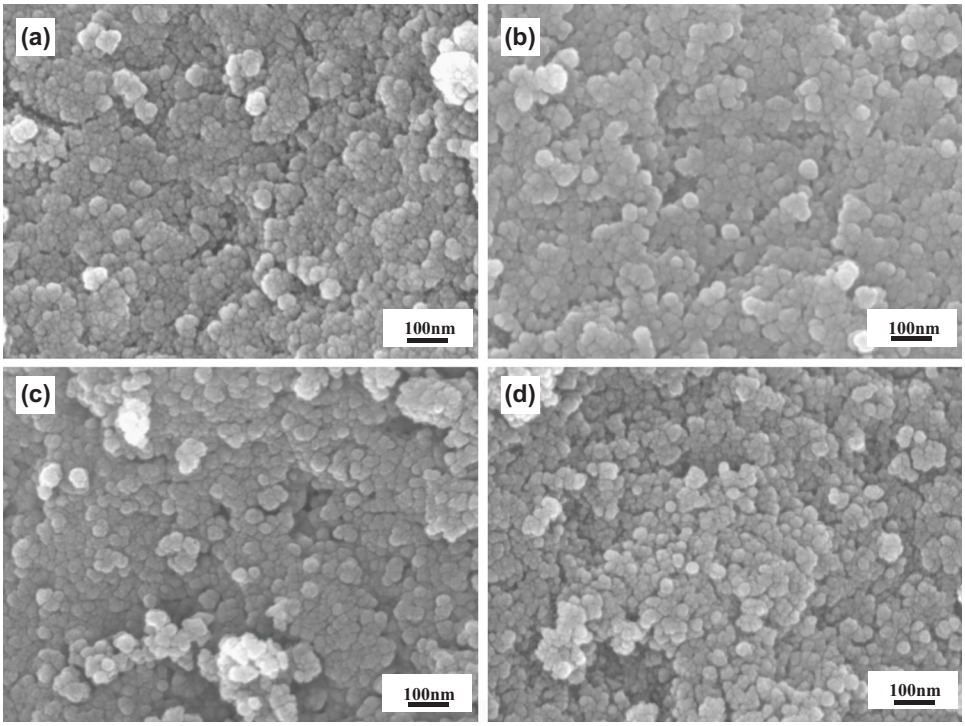


**Fig. 5** SEM images of the $SiO_2$–$W_xTiO_2$ composite aerogels synthesized with different solvothermal parameters and W/Ti molar ratio: **a** $SiO_2$–2mol%$W_xTiO_2$, 100 °C, 3 h; **b** $SiO_2$–2mol%$W_xTiO_2$, 100 °C, 27 h; **c** $SiO_2$–1mol%$W_xTiO_2$, 180 °C, 3 h; **d** $SiO_2$–5mol%$W_xTiO_2$, 180 °C, 3 h

followed by freeze drying. It can be found that the pure $SiO_2$ aerogel after freeze drying consists of $SiO_2$ nanoparticles about 10 nm and lots of pores about 20 nm consistent with the width of BC due to its complete hydrolysis during the solvothermal process. As shown in Fig. 6c, d, the $SiO_2$–2mol%$W_xTiO_2$ composite aerogel consists of bigger particles and smaller pores than the pure $SiO_2$ aerogel. It is reasonable that after the $SiO_2$–BC precursor gel soaked with the mixed solution of $H_2WO_4$/$TiCl_4$ underwent the process of solvothermal crystallization, the $W_xTiO_2$ nanoparticles were deposited in the network structure of the gel, which caused a certain degree of decrease of the pore size in the aerogels. In the high-resolution transmission electron microscopy image of the composite aerogel, the characteristic crystal lattice spacing of 0.35 nm is observed, corresponding to the (101) plane of anatase $TiO_2$, which means that the anatase $TiO_2$ crystals is embedded in the porous network of the composite aerogels.

Figure 7 shows the schematic diagram of the formation mechanism of the $SiO_2$–$W_xTiO_2$ composite aerogels with solvothermal crystallization and freeze drying method. When the precursor BC–$SiO_2$ gel soaked with the mixed $H_2WO_4$/$TiCl_4$ solution underwent the process of solvothermal crystallization, firstly large number of polar groups (–OH) on the surface of BC would attract the $W_xTiO_2$ nanoparticles to deposit. With the advance of solvothermal reaction, the $W_xTiO_2$ nanoparticles continuously deposited, accompanied with crystallization and growing up. In the meantime, the BC was rapidly hydrolyzed under the condition of strong acid, high temperature and pressure, forming cellotetrose, cellotriose, cellobiose, and the final product of D-(+)-glucose (see Eq. 1). The space left by hydrolysis of BC is beneficial to the increase of pore volume of the composite aerogels, at the same time, the polysaccharide produced by hydrolysis of BC promoted further the deposition of $W_xTiO_2$ particles. Therefore, in this study, the presence of BC in the composite gel and the hydrolysis of BC during the solvothermal process played a role in adjusting and improving the porous network structure and crystallization of the composite aerogels. It is because of the role of the BC which was used as an expanding agent and induced the deposition and crystallization of particles during the solvothermal crystallization process that the $SiO_2$–$W_xTiO_2$ composite aerogels prepared by freeze drying exhibit higher $TiO_2$ content and porous structure with high pore volume. So the as-prepared composite aerogels are expected to exhibit higher adsorption and photocatalytic degradation efficiency for organic pollutants.

$$(C_6H_{10}O_5)_n \xrightarrow[H^+]{H_2O} (C_6H_{10}O_5)_4 \xrightarrow[H^+]{H_2O} (C_6H_{10}O_5)_3 \xrightarrow[H^+]{H_2O} C_{12}H_{22}O_{11} \xrightarrow[H^+]{H_2O} C_6H_{12}O_6 \quad (1)$$

Figure 8a shows the $N_2$ adsorption–desorption isotherms of the synthesized $SiO_2$–$W_xTiO_2$ composite aerogels. All the curves of the composite aerogels with different W/Ti molar ratio accord with the characteristics of IV type in IUPAC classification with obvious hysteresis loop, which

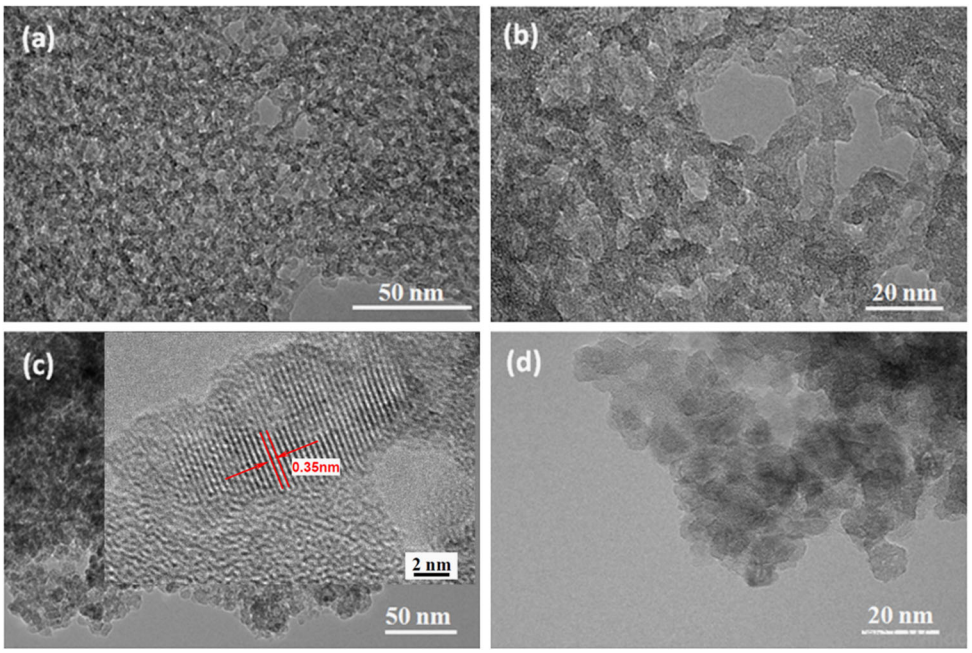


**Fig. 6** TEM images of the composite aerogels: **a**, **b** $SiO_2$ aerogel without $W_xTiO_2$ deposition; **c**, **d** $SiO_2$–2mol% $W_xTiO_2$ composite aerogels with solvothermal crystallization for 3 h at 180 °C (*inset* is the HRTEM image of the composite aerogel)

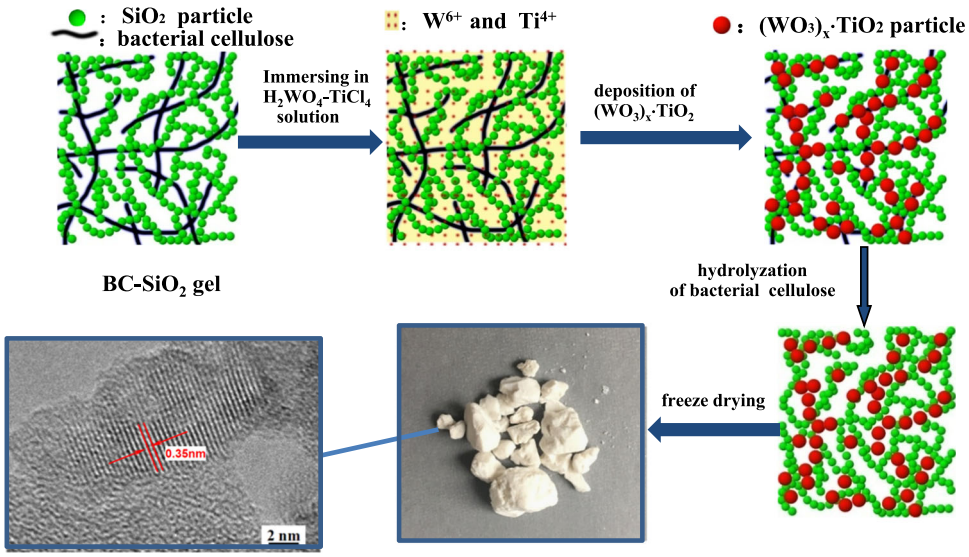


**Fig. 7** Schematic diagram of the formation mechanism of the $SiO_2$–$W_xTiO_2$ composite aerogels with solvothermal crystallization and freeze drying method

indicate that the prepared $SiO_2$–$W_xTiO_2$ composite aerogels have typical characteristics of mesoporous materials. The pore size distribution profiles of the composite aerogels are shown in Fig. 8b. It can be seen that the pore size is mostly in the range of 3–7 nm for the composite aerogels. With the increase of W/Ti molar ratio, the pore size of the composite aerogels decreased gradually. The BET analysis results and crystal phase of the $SiO_2$–$W_xTiO_2$ composite aerogels are shown in Table 1. It can be found that the specific surface area of the composite aerogels is in the range of 297 –377 $m^2/g$, and the pore volume decreases with the increase of W/Ti mol%, indicating that the incorporation of W will affect the pore structure of the composite aerogels to a certain extent. In our previous work [32], the as-prepared composite aerogels using different cellulose as templates was compared. It was found that the BC-derived composite aerogel has higher pore volume and pore size than that of without template. Moreover, the composite aerogel with BC as template has the biggest pore size, much bigger than that of the aerogel synthesized with nano-cellulose as template. During the gelatinization, BC will form a cross chain structure with $SiO_2$ gel, and the complete network structure containing BC chains may still be retained partly after solvothermal crystallization process, which is favorable for

forming porous structure. Therefore, it is concluded that BC is an ideal template for synthesizing porous composite aerogel materials.

The UV–Vis absorption spectra and $(Ah\nu)^{1/2}$–$h\nu$ relationship of the composite aerogels with different W/Ti molar ratio are shown in Fig. 9. As is shown in Fig. 9b, the band gap of the prepared composite aerogels is between 2.82–2.88 eV, which is lower than 3.2 eV of P25. This result indicates that incorporation of W can reduce the band gap of the composite aerogel, which is favorable for its achieving excellent photocatalytic performance under visible light irradiation with lower energy apart from the the UV irradiation with higher energy.

Figure 10a shows the adsorption/photocatalytic performance for RhB of the synthesized $SiO_2$–2mol%$W_xTiO_2$ composite aerogels with solvothermal crystallization at 100 °C for different time. It can be seen that the adsorption/visible light photocatalytic activity of the composite aerogels was significantly improved with the extension of the solvothermal time. The reason is that with the extension of

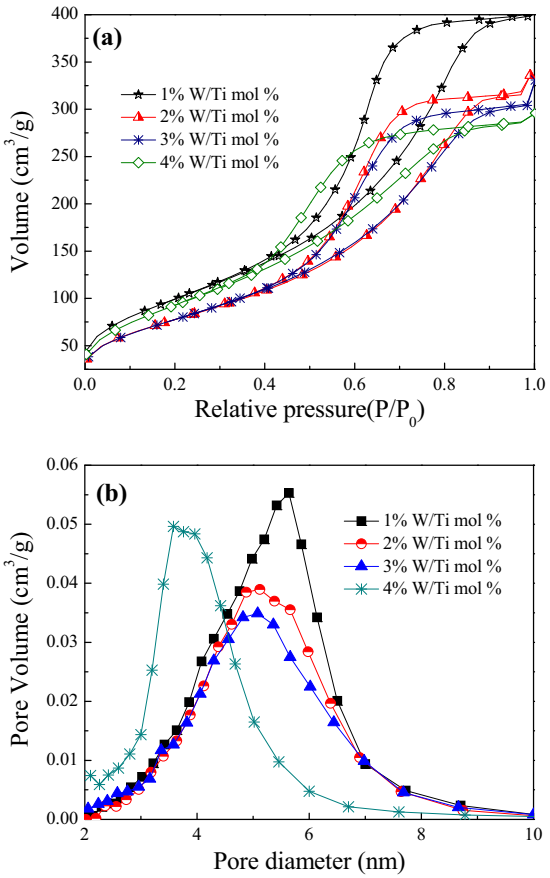


**Fig. 8** $N_2$ adsorption-desorption isotherm **a** and pore size distribution **b** of the $SiO_2$–$W_xTiO_2$ composite aerogels with solvothermal crystallization for 3 h at 180 °C and different W/Ti molar ratio

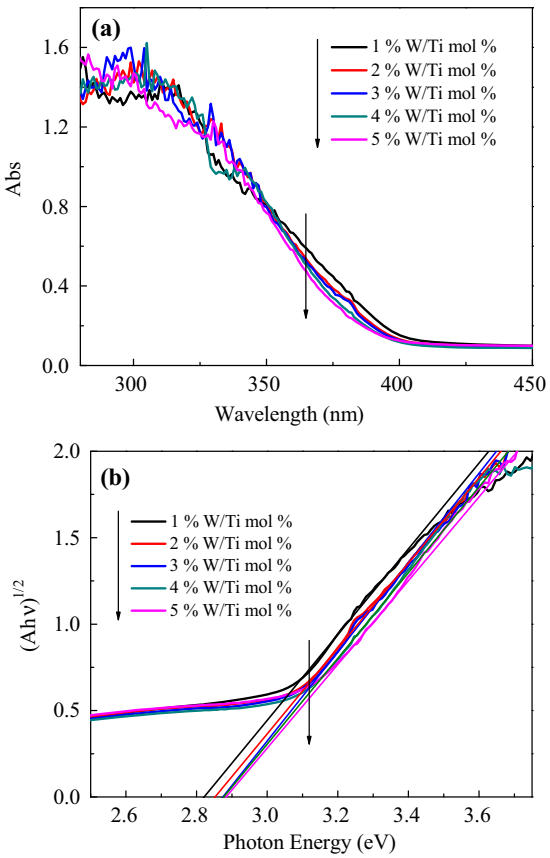


**Fig. 9** UV–Vis absorption spectra **a** and $(Ah\nu)^{1/2}$–hν relationship derived from the absorption spectra **b** of the $SiO_2$–$W_xTiO_2$ composite aerogels with solvothermal crystallization for 3 h at 180 °C and different W/Ti molar ratio

**Table 1** The BET analysis results and crystal phase of the obtained $SiO_2$–$W_xTiO_2$ composite aerogels with solvothermal crystallization for 3 h at 180 °C and different W/Ti molar ratio

| W/Ti mol% | Solvothermal temperature and time (°C/h) | Specific surface area ($m^2$/g) | Pore diameter (nm) | Pore volume ($cm^3$/g) | Crystal phase |
|---|---|---|---|---|---|
| 1 | 180/3 | 377 | 7.00 | 0.660 | Anatase $TiO_2$ |
| 2 | 180/3 | 297 | 7.02 | 0.522 | Anatase $TiO_2$ |
| 3 | 180/3 | 301 | 6.80 | 0.515 | Anatase $TiO_2$ |
| 4 | 180/3 | 359 | 5.14 | 0.460 | Anatase $TiO_2$ |

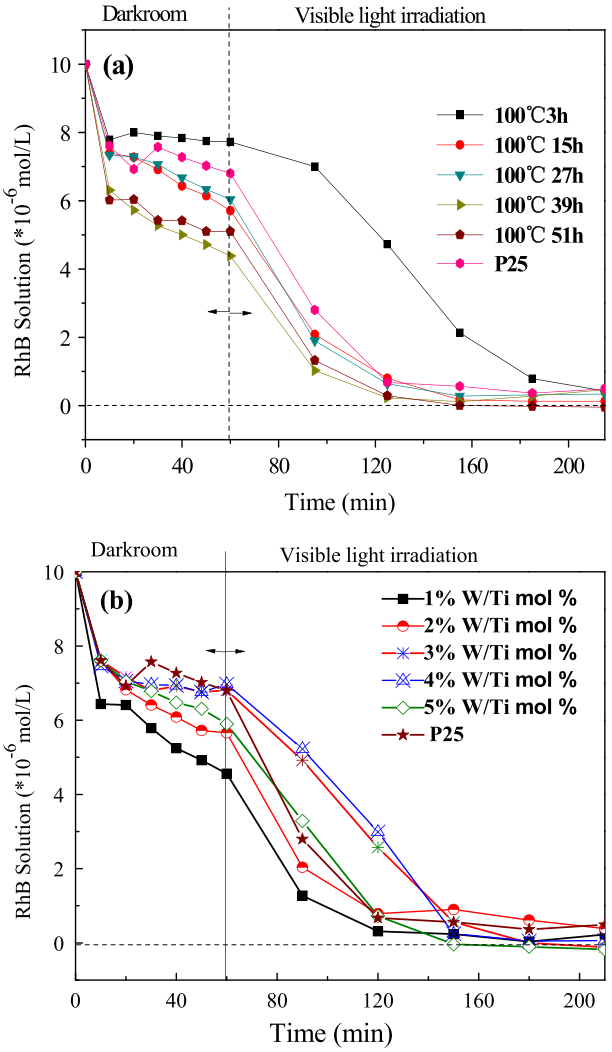


**Fig. 10** The adsorption/photocatalytic degradation curves for RhB of the $SiO_2$–$W_xTiO_2$ composite aerogels synthesized under different conditions **a** solvothermal crystallization at 100 °C for different time with W/Ti mol% = 2%; **b** solvothermal crystallization at 180 °C for 3 h with different W/Ti mol%

solvothermal time, the BC hydrolysis proceeds more completely with leaving larger amount of pores, which provided the composite aerogels with better adsorption. In addition, with the increase of the solvothermal time, the deposition amount and crystallinity of $W_xTiO_2$ nanoparticles were increased, enhancing the adsorption/visible light photocatalytic ability of the composite aerogels for RhB. Compared with P25 powder, the adsorption/photocatalytic performance of the composite aerogels was all higher than that of P25 except the sample with solvothermal 3 h, which indicates that the synergy of adsorption and photocatalysis of the composite aerogels is favorable for improving the removal efficiency of organic pollutants in wastewater.

The adsorption/photocatalytic degradation curves for RhB of the $SiO_2$–$W_xTiO_2$ composite aerogels by solvothermal crystallization for 3 h at 180 °C with different W/Ti molar ratio are shown in Fig. 10b. It can be seen that all of the prepared composite aerogels have good adsorption performance for RhB, and the adsorption rate of the composite aerogel with 1% W/Ti mol% reached 54.4% in 60 min. With the increase of W/Ti mol%, the adsorption capacity tended to decrease owing to the decrease of the pore volume as is shown in Table 1. It is obvious that the adsorption capacity of the composite aerogels was higher than that of the P25 powder (32.1% in 60 min) due to the high specific surface area and pore volume. In addition, the composite aerogels with 1 and 2% W/Ti mol% exhibit best adsorption/photocatalytic properties, with the total adsorption/photocatalytic degradation efficiency for RhB attaining to 96.8% with 120 min.

## 4 Conclusion

The $SiO_2$–$W_xTiO_2$ composite aerogels were synthesized by solution immersion, solvothermal crystallization and freeze-drying method using $SiO_2$–BC gel as precursor skeleton. The prepared composite aerogels have higher specific surface area with 297–377 $m^2 g^{-1}$ and pore volume with 0.46–0.66 $cm^3 g^{-1}$, and the main crystalline phase is the i anatase $TiO_2$ with higher crystallinity. The presence and hydrolysis of BC as a template and inducer during the solvothermal process played an important role in enhancing the porous network structure of the composite aerogels and inducing the deposition/crystallization of $W_xTiO_2$ nanoparticles.

The adsorption/visible photocatalytic degradation efficiency for the organic dye (RhB) of the composite aerogels was significantly higher than that of pure P25 powder. Doping of 2–3% W and increasing the solvothermal crystallization time are favorable for improving the adsorption/photocatalytic performance of the composite aerogels. Therefore, the $SiO_2$–$W_xTiO_2$ composite aerogels in this study had a broad prospect to be used as a high efficient photocatalyst in the field of wastewater treatment and air purification.

**Acknowledgements** This work was financially supported by the National Natural Science Foundation of China (No. 51278074), the 2015 Science & Technology Project by the Ministry of Housing and Urban-Rural Development of China (2015-K1-042), the 2015 Liaoning Province Colleges and Universities Outstanding Talent Support Program (LR2015005), the project of Dalian Science & Technology Foundation (2015B11NC074) and Dalian City Construction Science & Technology Project (201612).

**Compliance with ethical standards**

**Conflict of interest** The authors declare that they have no competing interests.

## References


1. Sabry RS, Al-Haidarie YK, Kudhier MA (2016) Synthesis and photocatalytic activity of TiO2 nanoparticles prepared by sol–gel method. J Solgel Sci Technol 78(2):299–306
2. Li H, Liu B, Yin S, Sato T, Wang Y (2015) Visible light-driven photocatalytic activity of oleic acid-coated TiO2 nanoparticles synthesized from absolute ethanol solution. Nanoscale Res Lett 10:415
3. Sun B, Zhou G, Yan Z, Liu R, Li T (2015) Photocatalytic properties of exposed crystal surface-controlled rutile TiO2 nanorod assembled microspheres. Chem Eng J 264:125–133
4. Wu MC, Lee PH, Lee DL (2015) Enhanced photocatalytic activity of palladium decorated TiO2 nanofibers containing anatase-rutile mixed phase. Int J Hydrogen Energy 40:4558–4566
5. Ren L, Li Y, Hou J, Zhao X, Pan C (2014) Preparation and enhanced photocatalytic activity of TiO2 nanocrystals with internal pores. ACS Appl Mater Interfaces 6:1608–1615
6. Li N, Zhang X, Yuan S, Zhang X, Yuan Y, Li X (2015) hollow Au-Ag nanoparticles)-TiO2 composites for improved photocatalytic activity prepared from block copolymer-stabilized bimetallic nanoparticles. Phys Chem Chem Phys 17:12023–12030
7. Wu X, Yin S, Dong Q, Guo C, Kimura T, Matsushita J, Sato T (2013) Photocatalytic properties of Nd and C codoped TiO2 with the whole range of visible light absorption. J Phys Chem C 117:8345–8352
8. Li H, Yin S, Wang Y, Sato T (2013) Efficient persistent photocatalytic decomposition of nitrogen monoxide over a fluorescence-assisted CaAl2O4:(Eu, Nd)/(Ta,N)-codoped TiO2/Fe2O3. Appl Catal B 132-133:487–492
9. Kim JY, Kim CS, Chang HK, Kim TO (2010) Effects of ZrO2 addition on phase stability and photocatalytic activity of ZrO2/TiO2 nanoparticles. Adv Powder Technol 21:141–144
10. Luan P, Xie M, Fu X, Qu Y, Sun X, Jing L (2015) Improved photoactivity of TiO2-Fe2O3 nanocomposites for visible-light water splitting after phosphate bridging and its mechanism. Phys Chem Chem Phys 17:5043–5050
11. Riboni F, Bettini LG, Bahnemann DW, Selli E (2013) WO3-TiO2 vs.TiO2 photocatalysts: effect of the W precursor and amount on the photocatalytic activity of mixed oxides. Catal Today 209:28–34
12. Zhang L, Li Y, Zhang Q, Wang H (2013) Hierarchical nanostructure of WO3 nanorods on TiO2 nanofibers and the enhanced visible light photocatalytic activity for degradation of organic pollutants. Crystengcomm 15:5986–5993
13. Ramos-Delgado NA, Gracia-Pinilla MA, Maya-Treviño L, Hinojosa-Reyes L, Guzman-Mar JL, Hernández-Ramírez A (2015) Solar photocatalytic activity of TiO2 modified with WO3 on the degradation of an organophosphorus pesticide. J Hazard Mater 263:36–44
14. Yan M, Li G, Guo C, Guo W, Ding D, Zhang S (2016) WO3-x sensitized TiO2 sphere with full-spectrum-driven photocatalytic activities from UV to near infrared. Nanoscale 8:17828–17835
15. Shi F, Liu J, Huang X, Yu L, Liu S, Feng X, Fan C (2015) Hydrothermal synthesis of mesoporous WO3-TiO2 powders with enhanced photocatalytic activity. Adv Powder Technol 26:1435–1441
16. He S, Bi Y, Zhang Y, Cao H, Shi X, Luo X, Zhang L (2015) One-pot synthesis and characterization of acid-catalyzed melamine formaldehyde/SiO2 aerogel via sol–gel technology. J Solgel Sci Technol 74:175–180
17. Cui S, Cheng W, Shen X, Fan M, Russell A, Wu Z, Yi X (2011) Mesoporous amine-modified SiO2 aerogel: a potential CO2 sorbent. Energy Environ Sci 4:2070–2074
18. Lin B, Ruan J, Cui S, Shen X, Yu S (2015) A new type of super hydrophilic SiO2 aerogel for use as a potential NH3 sorbent. Curr Nanosci 11:120–128
19. Zu G, Shen J, Wang W, Zou L, Xu W, Zhang Z (2015) Preparation of heat-resistant, core/shell nanostructured TiO2/SiO2 composite aerogels and their photocatalytic properties. Acta Physico-Chimica Sinica 31:360–368
20. Rankin JM, Baker S, Klabunde KJ (2014) Mesoporous aerogel titanium oxide–silicon oxide combinations as adsorbents for an azo-dye. Microporous Mesoporous Mater 190:105–108
21. Yu Y, Zhu M, Liang W, Rhodes S, Fang J (2015) Synthesis of silica–titania composite aerogel beads for the removal of Rhodamine B in water. Rsc Adv 5:72437–72443
22. Liu J, Wang X, Shi F, Yu L, Liu S, Hu S, Liu D (2016) Synthesis of mesoporous SiO2 aerogel/WxTiO2 nanocomposites with high adsorptivity and photocatalytic activity. Adv Powder Technol 27:1781–1789
23. Zhang HX, He XD, He F (2009) Microstructural characterization and properties of ambient-dried SiO2 matrix aerogel doped with opacified TiO2 powder. J Alloys Comp 469:366–369
24. Zhang F, Sun D, Yu C, Yin Y, Dai H, Shao G (2015) A sol–gel route to synthesize SiO2/TiO2 well-ordered nanocrystalline mesoporous photocatalysts through ionic liquid control. New J Chem 39:3065–3070
25. Wang X, Liu J, Shi F, Liu S, Feng X, Bao L (2014) Influences of heat-treatment on the microstructure and properties of silica–titania composite aerogels. J Porous Mater 21:293–301
26. Zu G, Shen J, Wang W, Zou L, Lian Y, Zhang Z (2015) Silica–titania composite aerogel photocatalysts by chemical liquid deposition of titania onto nanoporous silica scaffolds. ACS Appl Mater Interfaces 7:5400–5409
27. Russler A, Wieland M, Bacher M, Henniges U, Miethe P, Liebner F, Potthast A, Rosenau T (2012) Akd-modification of bacterial cellulose aerogels in supercritical CO2. Cellulose 19:1337–1349
28. Sai H, Fu R, Xing L, Xiang J, Li Z, Li F, Zhang T (2015) Surface modification of bacterial cellulose aerogels' web-like skeleton for oil/water separation. Acs Appl Mater Interfaces 7:7373–7381
29. Pircher N, Veigel S, Aigner N, Nedelec JM, Rosenau T, Liebner F (2014) Reinforcement of bacterial cellulose aerogels with biocompatible polymers. Carbohydr Polym 111:505–513
30. Sai H, Xing L, Xiang J, Cui L, Jiao J, Zhao C, Li Z, Li F (2013) Flexible aerogels based on an interpenetrating network of bacterial cellulose and silica by a non-supercritical drying process. J Mater Chem A 1:7963–7970
31. Olsson RT, Azizi Samir MA, Salazaralvarez G, Belova L, Ström V, Berglund LA, Ikkala O, Nogués J, Gedde UW (2010) Making flexible magnetic aerogels and stiff magnetic nanopaper using cellulose nanofibrils as templates. Nat Nanotechnol 5:584–588
32. Shi F, Yu T, Hu S, Liu J, Yu L, Liu S (2016) Synthesis of highly porous SiO2-(WO3)x·TiO2 composite aerogels using bacterial cellulose as template with solvothermal assisted crystallization. Chem Eng J 292:105–112